ACS Catalysis

pubs.acs.org/acscatalysis

Research Article

Accelerating Chemo- and Regioselective Hydrogenation of Alkynes over Bimetallic Nanoparticles in a Metal−Organic Framework

Luyan Li, Weijie Yang, Qihao Yang, Qiaoqiao Guan, Junling Lu, Shu-Hong Yu, and Hai-Long Jiang*

Cite This: *ACS Catal.* 2020, 10, 7753−7762

Read Online

ACCESS | Metrics & More | Article Recommendations | Supporting Information

ABSTRACT: Selective semihydrogenation of alkynes has been a long-term and significant target, yet it remains a great challenge. Herein, bimetallic nanoparticles in a metal−organic framework (MOF), i.e., CuPd@ZIF-8 composite, featuring a cubic CuPd core and a porous ZIF-8 shell, have been rationally fabricated for this end. Given the unique physicochemical properties, the Cu nanocubes can not only convert solar energy into heat to accelerate the reaction but also serve as the seed for *in situ* formation of Pd nanoparticles (NPs) on their external surface to regulate the chemoselectivity of Pd active sites. The additional growth of the MOF shell is helpful to stabilize the CuPd core and offer regioselectivity via the steric hindrance effect. Ammonia borane provides active hydrogen species to significantly boost the hydrogenation and ensure the high selectivity. As a result, the CuPd@MOF exhibits high efficiency, featuring a turnover frequency (TOF, 6799 min^{-1}) of 5−10^5 times higher than that in previous reports, and high chemo- and regioselectivity toward the semihydrogenation of alkynes, in the presence of NH_3BH_3 as a hydrogen source, under visible-light irradiation at ambient temperature.

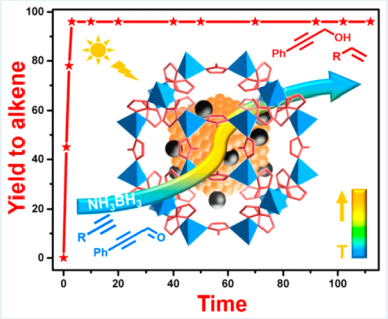

KEYWORDS: *metal−organic framework, photothermal effect, alloy nanocrystals, plasmonic, selective catalysis*

INTRODUCTION

Selective semihydrogenation of alkynes to alkenes is of great importance and has attracted particular attention in both academia and the chemical industry, especially relevant to commodity chemical production (e.g., purification of phenylethylene feeds for polymerization). Typically, the alkynes, especially terminal alkynes, are prone to overhydrogenation to alkanes because of their high reactivity; the selective semihydrogenation of alkynes remains a particular challenge.[1−10] To date, heterogeneous selective semihydrogenation reactions have been generally investigated with metal-based catalysts in a hydrogen (H_2) atmosphere. Among them, Pd-based bimetallic catalysts are suggested to be most promising for this reaction. The classical Lindlar catalyst, partially poisoning Pd with a secondary metal such as Pb to improve selectivity, remains the choice in industry. However, the toxic lead, unsatisfied activity, and high price are the driving forces for the search of alternative catalysts. With the research effort, CuPd has been found based on theoretical simulations to be very promising owing to its nontoxicity and high selectivity for hydrogenation reactions.[11,12] Unfortunately, experimental reports show that the semihydrogenation reaction over CuPd usually requires high H_2 pressure and still causes overhydrogenation to alkanes at high conversion in the prolonged reaction time.[1,13−15] Therefore, surpassing the limitation of the long-term "trade-off" effect to efficiently produce alkenes with constant selectivity at high conversion level still poses a challenge by using the CuPd catalysts, especially under ambient/moderate pressure, which is highly desired.

On the other hand, the increase of reaction temperature is a general way to accelerate the kinetics of catalytic reactions. From the viewpoint of energy saving, the conversion of solar radiation into heat energy, via the localized surface plasmon resonance (LSPR) of metal catalysts,[16−19] to elevate the reaction temperature is desirable. Although Cu nanoparticles (NPs) possess an LSPR-induced photothermal effect, it is rarely reported because they are easily oxidized and/or chemically etched during the reaction/illumination.[20] To address this issue, encapsulating Cu NPs into a porous material with appropriate pore sizes has been shown to be an advisable solution.[21] The porous shell will not only prevent the Cu NPs from being further oxidized or etched during the reaction, to some extent, but also facilitate the enrichment of substrates. Moreover, a uniform pore size might give rise to size-/regioselective catalysis via the steric hindrance effect. To meet these requirements, metal−organic frameworks (MOFs),[22−30] a relatively new class of crystalline porous materials with high surface area and tunable pore sizes, might be ideal candidates.[31−48]

Bearing the above considerations in mind, we have rationally fabricated a core−shell structured MOF composite, namely,

Received: January 11, 2020
Revised: June 6, 2020
Published: June 11, 2020

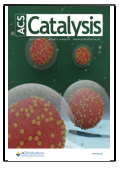

CuPd@ZIF-8, which features cubic Cu supported Pd NPs together as a core and a representative MOF, ZIF-8 (Zn(2-methylimidazole)$_2$),[49,50] as a shell (Scheme 1). Particularly, to

Scheme 1. Schematic Illustration Showing the Preparation Process of CuPd@ZIF-8

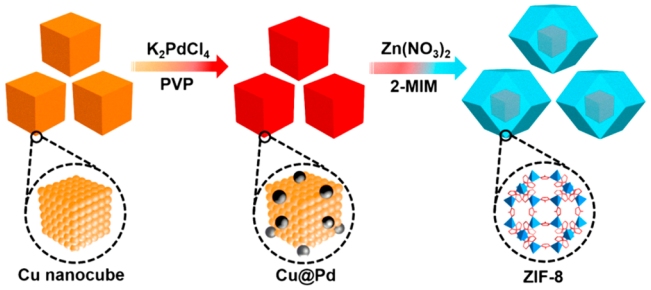

avoid high-pressure H_2 gas and tune the selective hydrogenation, ammonia borane (NH_3BH_3), as a particular hydrogen source, has been introduced into the alkyne hydrogenation system. Thanks to the plasmon-driven photothermal effect of Cu nanocubes (NCs), the high Pd activity boosted by active hydrogen species from NH_3BH_3, the chemoselectivity influenced by Cu−Pd interaction while being dominated by the NH_3BH_3 hydrogen source, and the protection and steric hindrance effect of the ZIF-8 shell, the CuPd@ZIF-8 composite exhibits excellent activity, both chemo- and regioselectivity without the "trade-off" effect, as well as good recyclability, for alkyne semihydrogenation under visible-light irradiation at ambient temperature. Remarkably, the turnover frequency (TOF) of phenylacetylene semihydrogenation reaches 6799 min^{-1}, surpassing all previously reported metal-based catalysts, and the high selectivity can be well maintained with extended reaction time. Based on our knowledge of the literature, this is an unusual report on a heterogeneous catalyst with high activity and chemo- and regioselectivity toward hydrogenation of alkynes.

RESULTS AND DISCUSSION

The Cu NCs were prepared in H_2O in the presence of $CuCl_2 \cdot 2H_2O$, glucose, and hexadecylamine (HAD).[51] The Pd NPs were formed on the external surface of Cu NCs to give CuPd NCs via the galvanic reaction between Pd^{2+} and Cu^0 ($E_{Pd^{2+}/Pd}$ = +0.951 eV vs SHE; $E_{Cu^{2+}/Cu}$ = +0.337 eV vs SHE). Following that, the Zn^{2+} and 2-methylimidazole were assembled onto the surface of CuPd NCs with the help of interfacing polyvinyl pyrrolidone (PVP), leading to the formation of core−shell structured CuPd@ZIF-8 composites (Scheme 1).

The powder X-ray diffraction (XRD) pattern of CuPd NCs shows two peaks at 43.5° and 50.7°, which can be assigned to the (111) and (200) diffractions of face-centered cubic Cu, respectively, indicating the successful synthesis of Cu NCs (Figure S1a). The absence of an identifiable diffraction peak of Pd indicates the possibly low Pd content and/or small Pd sizes. The powder XRD pattern of CuPd@ZIF-8 clearly demonstrates the formation of ZIF-8 with good crystallinity (Figure S1a). N_2 sorption of CuPd@ZIF-8 indicates its high Brunauer−Emmett−Teller (BET) surface area (1077 m^2/g) and typical microporous character (Figure S1b). The slight decrease in surface area compared to parent ZIF-8 (1296 m^2/g) is ascribed to the mass occupation of CuPd NCs.

The scanning electron microscopy (SEM) observation shows that the Cu NCs have a regular shape with average sizes of 61 ± 6 nm (Figure 1a). Transmission electron

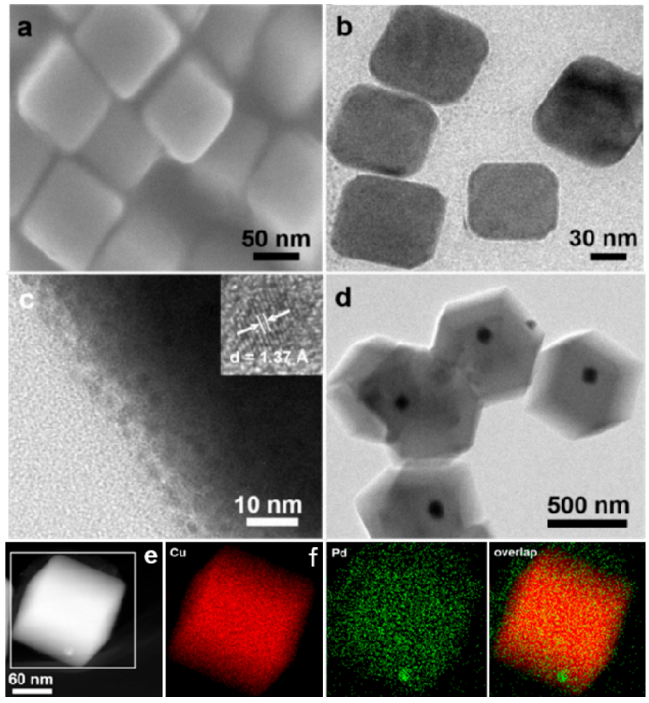

Figure 1. (a) SEM image of Cu NCs. TEM images of (b, c) CuPd NCs and (d) CuPd@ZIF-8. Inset of c: HRTEM image of Pd NPs. (e) HAADF-STEM of CuPd and (f) the corresponding elemental mapping of Cu (red) and Pd (green).

microscopy (TEM), high-resolution TEM (HRTEM), and high-angle annular dark-field scanning TEM (HAADF-STEM) observation for CuPd NCs suggest that Pd NPs (~2.5 nm) are formed on the surface of Cu NCs and almost do not change the original morphology of the latter (Figure 1b,c,e, Figure S2a). Elemental mapping results further support the uniform Pd dispersion on the Cu NCs (Figure 1f). The well observable lattice fringe with spacing of 1.37 Å could be indexed to the (220) plane of Pd NPs (Figure 1c, inset). The TEM image of CuPd@ZIF-8 indicates that the CuPd NCs are well encapsulated by the ZIF-8 shell, and the size of an individual CuPd@ZIF-8 particle is 600−1000 nm (Figure 1d, Figure S2b). The actual contents of Cu and Pd are determined to be 5.5 and 0.1 mol %, respectively, in the CuPd@ZIF-8 composite by inductively coupled plasma atomic emission spectroscopy (ICP-AES). The trace Pd loading signifies the low cost of this catalyst. Notably, the LSPR-induced absorption of Cu NCs in 575−700 nm can be well inherited to the CuPd@ZIF-8 composite (Figure S3), suggesting that the ZIF-8 shell can be successfully penetrated by light irradiation. To investigate the interaction between Pd and Cu, the temperature-programmed reduction (TPR) for CuPd@ZIF-8 was conducted. Two reduction peaks at around 160 and 340 °C can be assigned to the oxidative species of PdO and Cu_2O,[14] respectively (Figure 2a). Apparently, the reduction temperature of Cu_2O at ~340 °C for CuPd@ZIF-8 is lower than that (369 °C) for Cu@ZIF-8, revealing the interaction between Pd and Cu. The reduction of Cu_2O in CuPd@ZIF-8 might be promoted by the H_2 spillover from Pd to the neighboring Cu_2O.[52] This Cu−Pd interaction is further supported by X-ray photoelectron

https://dx.doi.org/10.1021/acscatal.0c00177
ACS Catal. 2020, 10, 7753−7762

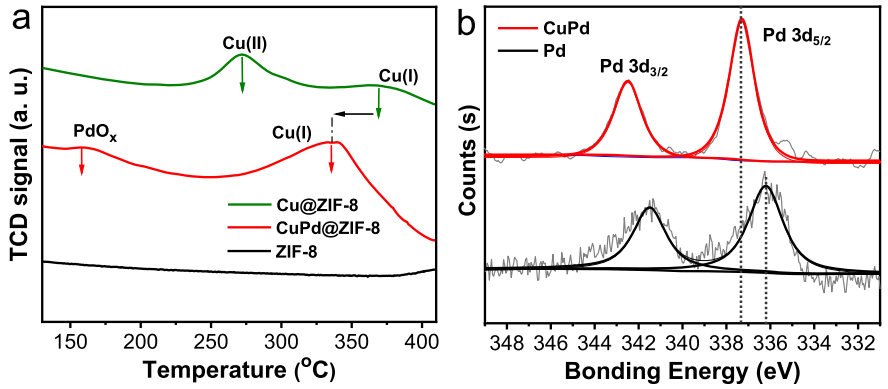

Figure 2. (a) TPR profiles for Cu@ZIF-8, CuPd@ZIF-8, and ZIF-8. (b) XPS spectra of Pd 3d.

spectroscopy (XPS) data. The $3d_{5/2}$ peak for Pd^0 shifts to the higher binding energy in CuPd due to the electron transfer from Pd to Cu, and the appearance of the Cu^{2+} peak would be due to the partial oxidation of Cu in CuPd NCs (Figure 2b, Figure S4).[19]

The above rationally fabricated CuPd@ZIF-8 composite is expected to afford an excellent performance toward selective hydrogenation of alkynes under light irradiation at ambient temperature. The phenylacetylene (**1a**) hydrogenation was first investigated to optimize the reaction parameters (Figure 3). As

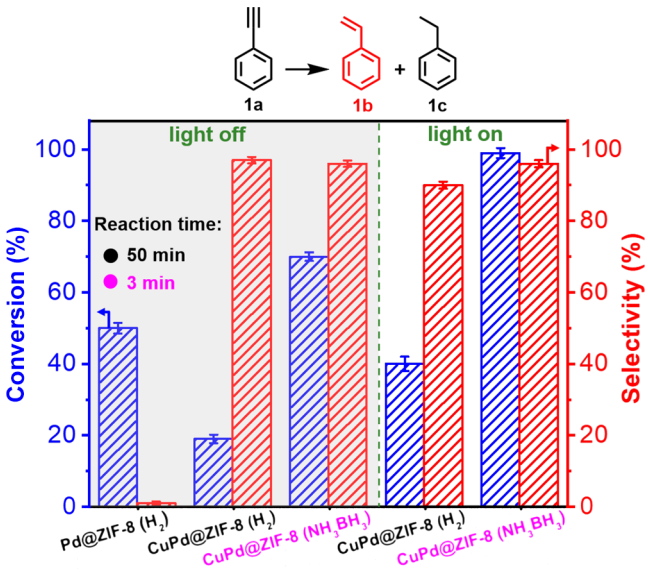

Figure 3. (a) Semihydrogenation of phenylacetylene in CH_3OH with a hydrogen donor of a H_2 balloon (or NH_3BH_3) over Pd@ZIF-8 (or CuPd@ZIF-8) in the absence (left side, with gray background) or presence (right side, no background) of light irradiation (>400 nm, 160 mW/cm^2).

expected, a high selectivity (97%) to phenylethylene (**1b**) can be achieved over CuPd@ZIF-8 in H_2 atmosphere at room temperature, which is distinctly different from the poor selectivity (<1%) over Pd@ZIF-8 (Figure 3, Figure S5). The results suggest that the introduction of Cu is crucial to the high selectivity, probably due to the lower adsorption stability between alkene and the formed Pd NPs outside Cu NCs.[1] Unfortunately, the conversion of **1a** over CuPd@ZIF-8 is only 19% under these conditions, which is even lower than Pd@ZIF-8, as the Cu introduction reduces the adsorption energy of substrates and suppresses the H_2 dissociation based on the previous reports.[1,53] The photothermal effect of Cu nanocubes in the catalyst is thought to be able to improve the conversion. To evaluate the efficiency of photothermal conversion of CuPd@ZIF-8, the temperature change in the solution along with time is detected. Results clearly show that light energy can be efficiently converted into heat in the presence of CuPd@ZIF-8 (Figure S6). As expected, by simply introducing light irradiation, the conversion of **1a** over CuPd@ZIF-8 can be promoted to 40%, reflecting the great contribution of the photothermal effect (Figure 3). While the activity is improved, the selectivity slightly decreases to 90% at this conversion (40%) and continues to fall off along with higher conversion (Figure S7), in the H_2 atmosphere. The results indicate that, with the contribution of the Cu−Pd interaction in CuPd@ZIF-8, the overhydrogenation trend might be hardly avoidable in the H_2 atmosphere, similar to the results in previous reports.[1,15]

The above results drive us to explore a suitable hydrogen source to afford constantly excellent selectivity at even high conversions toward the semihydrogenation of alkynes. Ammonia borane (NH_3BH_3) with a high hydrogen content of 19.6 wt % has been recognized as a highly potential hydrogen storage medium.[54−59] The NH_3BH_3 displays excellent solubility in methanol to *in situ* generate active hydrogen species, facilitating subsequent hydrogenation.[57−59] Therefore, it is assumed that NH_3BH_3 might be a suitable hydrogen source to meet this challenge. The alcoholysis of NH_3BH_3 over CuPd@ZIF-8 was found to steadily proceed, producing pure H_2, and the reaction can be promoted under the light irradiation (Figure S8). Encouraged by this, the semihydrogenation of **1a** was examined with NH_3BH_3 instead of H_2. Significantly, in reference to the 70% conversion of **1a**, light irradiation further leads to its almost complete conversion (99%) with 96% selectivity to **1b** within 3 min, based on the CuPd@ZIF-8 catalyst (Figure 3). This much higher activity than that using H_2 gas discussed above implies that NH_3BH_3 might generate special active hydrogen species to boost the reaction. In contrast, Pd@ZIF-8 gives only 68% selectivity, and no reaction occurs with ZIF-8, implying the importance of Pd for the activity and Cu for promoting the selectivity (Table S1). To our delight, the ZIF-8 shell almost does not effect the catalytic rate, based on the comparison of phenylacetylene hydrogenation kinetics over CuPd NCs and CuPd@ZIF-8 (Figure S9). The transport limitation of ZIF-8 has been further excluded by examining the yield dependence on the catalyst amount (Figure S10). The TOF of CuPd@ZIF-8 is calculated

https://dx.doi.org/10.1021/acscatal.0c00177
ACS Catal. 2020, 10, 7753−7762

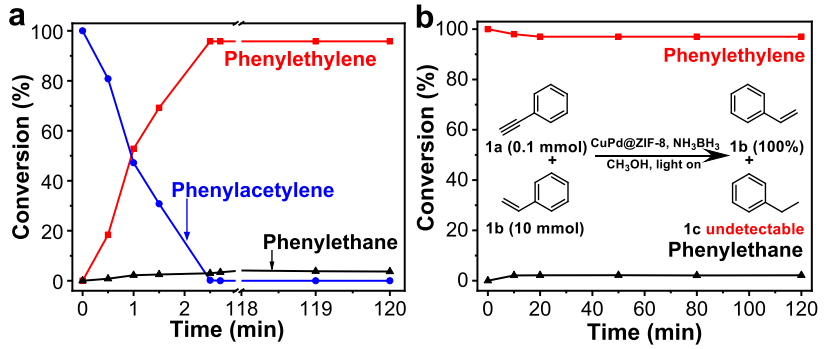

Figure 4. Time-dependent conversion of the hydrogenation of (a) phenylacetylene or (b) phenylethylene using CuPd@ZIF-8 with NH_3BH_3 as the hydrogen source under light irradiation at ambient temperature. Inset of b: selective reduction of a 1:100 mixture of phenylacetylene and phenylethylene.

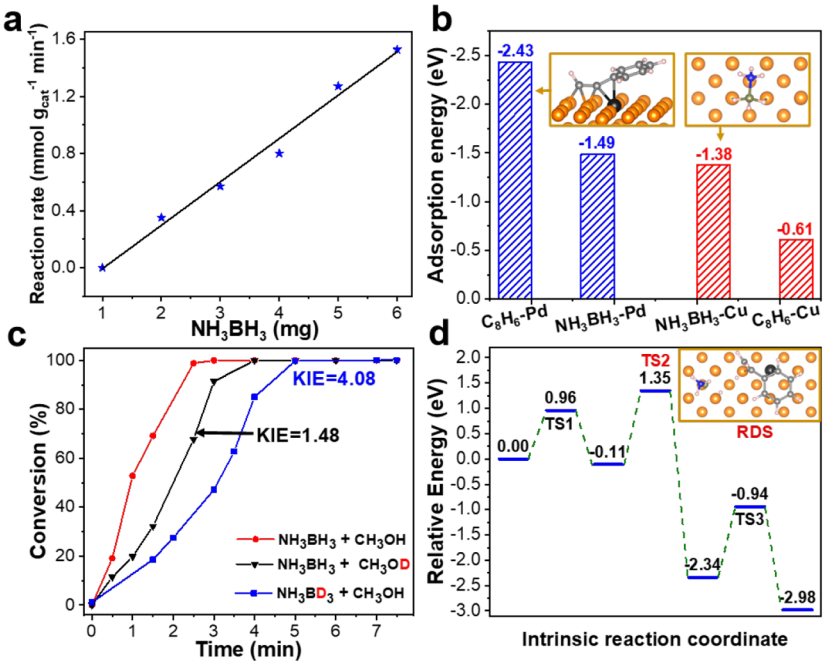

Figure 5. (a) Dependency of the reaction rate on the amount of NH_3BH_3. The correlation coefficient (R^2) is 0.98. (b) Adsorption energy of C_8H_6 and NH_3BH_3 on Pd and Cu sites, respectively. (c) Semihydrogenation of phenylacetylene using CuPd@ZIF-8 with NH_3BH_3 in CH_3OH (red), NH_3BH_3 in CH_3OD (black), and NH_3BD_3 in CH_3OH (blue). (d) Energies of intermediates and TSs in the mechanism of phenylacetylene hydrogenation to afford the 1st molecule of alkene (step I) over CuPd@ZIF-8 in the presence of NH_3BH_3 based on DFT calculations. Pd atom (black), Cu atom (orange).

to be 6799 min^{-1}, which represents the highest value among all reported metal catalysts for this reaction (Table S2). The high efficiency implies that the introduction of NH_3BH_3 might boost the conversion by the sufficient contact between the substrate and the hydrogen donor, which *in situ* generates hydrogen active species.[57]

More importantly, the selectivity shows an apparent decrease in the prolonged reaction time in the H_2 atmosphere, while almost no overhydrogenated product can be detected even when the reaction time length is extended to 2 h in the presence of NH_3BH_3 (Figure 4a, Figure S11). This point has been further clarified by employing **1b** as the reactant for hydrogenation over CuPd@ZIF-8, where almost no phenylethane (**1c**) can be produced (Figure 4b). The results unambiguously demonstrate that, in addition to the Cu in the catalyst, NH_3BH_3 also plays a critical role in the high chemoselectivity for the semihydrogenation of alkyne. Encouraged by these results, the experiment, the removal of a small amount of **1a** (0.1 mmol) from **1b** (10 mmol), which represents the important purification process in steam cracking of alkenes (usually containing a small fraction of alkyne impurities) in industry,[60,61] was investigated. Strikingly, **1a** can be completely converted to **1b** rapidly without overhydrogenation to **1c** (Figure 4b, inset). These results are very exciting and can be achieved in very few reports,[60,61] as the conventional catalysts (such as the commercial Lindlar catalyst) and/or hydrogen gas usually result in rapid overhydrogenation to alkanes with prolonged reaction time.

To gain insight into the hydrogenation process over the CuPd@ZIF-8 in the presence of NH_3BH_3, controlled experiments and density functional theory (DFT) calculations were carried out. The dependency of the reaction rate on the NH_3BH_3 amount toward the hydrogenation of **1a** suggests that it follows the first-order reaction, showing that NH_3BH_3 truly participated in the reaction (Figure 5a).[62] To understand the adsorption behavior of phenylacetylene (C_8H_6) and NH_3BH_3

https://dx.doi.org/10.1021/acscatal.0c00177
ACS Catal. 2020, 10, 7753−7762

substrates over the active sites, their adsorption on the catalyst surface has been investigated through calculating the adsorption energy and adsorption configuration (Figure 5b, Figure S12). The adsorption energy of C_8H_6 on the Pd site is −2.43 eV, apparently larger than that of NH_3BH_3 (−1.49 eV), which suggests the stronger interaction between C_8H_6 and Pd sites. Accordingly, C_8H_6 is preferentially adsorbed on Pd sites. In reverse, NH_3BH_3 is mainly adsorbed on Cu sites, due to its larger adsorption energy (−1.38 eV) than that of C_8H_6 (−0.61 eV) on Cu sites.

Subsequently, the deuterium-labeling experiments were conducted to figure out the real role of NH_3BH_3 in the reaction (Figures S13 and S14). Whatever NH_3BD_3 or ND_3BH_3 is introduced into CH_3OH, the deuterated phenylethylene can be obtained (Figure S14), clearly approving that the cleavage of both B−H and N−H bonds is involved in the reaction, and probably the generated hydrogen species ($H^{\delta-}$ and/or $H^{\delta+}$)[54] participate in the formation of phenylethylene product. Furthermore, the ratio (4.08) of rate constants, KIE (K_L/K_H), falls in the value range (2−7) of the primary kinetic isotope effect,[63] for the reactions involving light (K_L) and heavy (K_H) isotopically substituted ammonia borane (NH_3BD_3), demonstrating that the activation of the B−H bond is the rate-determining step (RDS) in the reaction and revealing that the generated $H^{\delta-}$ might be involved in the reaction (Figure 5c). In contrast, the KIE of 1.48 for the reactions involving isotopically substituted methanol (CH_3OD) suggests that the O−H activation in methanol would not be the RDS in the reaction.

In sharp contrast to the deuterated NH_3BH_3 experiments above, no H−D exchange takes place, and all the H atoms in phenylethylene can be detected in the ^{1}H NMR spectrum with NH_3BH_3 in CD_3OD solvent (Figure S15), excluding the possibility of the H atom in the alkene product originating from CH_3OH. This is completely different from the reported *in situ* H_2 generation from NH_3BH_3 for the subsequent hydrogenation process in previous examples,[60,61] in which the H_2 originated from both B−H cleavage and the other proton in CH_3OH.[54] According to the reported work,[64] it is assumed that the active hydrogen species from B−H and N−H cleavage are able to react with the alkyne group directly to give the product, which is supported by the fact that negligible hydrogen gas production can be detected during our reaction (Figure S16).

For further clarity of how the hydrogenation process takes place, we propose a plausible mechanism by resorting to the DFT calculation and the above experimental results (Figures S17 and S18). It is proposed that the ideal alkyne hydrogenation in the presence of NH_3BH_3 involves three steps (I, II, III) and generates three molar alkenes by consuming one molar NH_3BH_3. The process (step I) of generating the first molecule of alkene has been confirmed by the DFT calculations. First of all, NH_3BH_3 and C_8H_6 are adsorbed onto the Cu and Pd surfaces, respectively. Then, the breaking of the B—H bond in NH_3BH_3 gives the first hydrogen species ($H^{\delta-}$) on the Cu surface, which nucleophilically attacks the C≡C bond (**TS1**) (Figure S17c). Meanwhile, the other H atom ($H^{\delta-}$) is also released by the second B—H breaking, coparticipating in the formation of the first molecule of alkene, which is identified as the RDS process with an energy barrier of 1.46 eV (**TS2**) (Figure 5d, Figure S17e). The new ammonia alkoxyborane complex (BH_2═NH_2) is subsequently created by transferring one H atom from —NH_3 to —BH (**TS3**), which is validated by the infrared spectroscopy (Figures S17g and S19). The second molecule of alkene is produced following a similar process as the first step (I) by consuming two $H^{\delta-}$ species from two B—H bond cleavages (Figures S17i−j and S18). The third molecule of alkene is generated via obtaining one H atom from the B—H breaking. It is supposed that the other proton is from the N—H breaking via an innersphere addition mechanism (Figure S18).[64] This assumption is supported by the deuterated experiments (ND_3BH_3 and CD_3OD), which indicate that the hydrogen species from N−H cleavage, but not the proton from CH_3OH, participates in the production of alkene (Figures S14 and S15). After producing the three molecules of alkene, $NH_4B(OCH_3)_4$ is accordingly generated, as made evident by the ^{11}B NMR spectrum for the mixture (Figure S20).

From the above experimental and calculated results, it is clear that the active hydrogen species ($H^{\delta-}$ and $H^{\delta+}$) from B−H and N−H cleavage directly react with alkynes instead of producing H_2. Given the weak interaction between the polar hydrogen species and alkenes,[62] the hydrogenation of alkenes is unfavorable, suppressing their overhydrogenation and thus resulting in high selectivity to alkenes. Therefore, such a hydrogenation process over CuPd@ZIF-8 is based on the reaction between **1a** and polar hydrogen species ($H^{\delta-}$ and $H^{\delta+}$) from NH_3BH_3, distinctly different from the reaction in the H_2 atmosphere.

To further investigate the stability and reusability of the catalyst, recycling experiments have been also carried out. To our delight, the activity of CuPd@ZIF-8 is well maintained in the five consecutive runs, indicating its great recyclability and stability (Figure S21a,b). In comparison, the conversion over CuPd NCs, in the absence of ZIF-8 shell protection, sharply decreases during the three cycles due to the surface oxidation and possible chemical etching of Cu NCs (Figure S21c,d).[20,31]

Encouraged by the outstanding catalytic performance of CuPd@ZIF-8 toward the semihydrogenation of phenylacetylene, a variety of alkynes with different functional groups have been investigated (Table 1). Delightedly, various terminal aryl alkynes with electron-donating (−OCH_3 and −CH_3) or electron-withdrawing (−F) substituents can be completely transformed to the corresponding alkenes with high chemoselectivity (>94%) (entries 1−5). Moreover, the selective hydrogenation of aliphatic alkynes can be also achieved with excellent selectivity (>94%), indicating the great substrate tolerance of the catalyst (entries 6−9). On the contrary, the hydrogenation of diphenylacetylene was greatly restrained, and only 7% conversion is achieved over CuPd@ZIF-8 (entry 10). The result indicates that the transformation of internal alkynes to the corresponding alkenes is impeded possibly due to the steric hindrance by the small pore size of ZIF-8, which makes the internal carbon−carbon triple bond hardly accessible to the Pd active sites. Inspired by this, the hydrogenation of the substrate with multiple functional groups, phenylpropiolaldehyde, is attempted to obtain the alkynol, 2-propyn-1-ol, which is an important corrosion inhibitor in the petrochemical industry (Table 2).[65] Incredibly, the desired product is obtained with 98% selectivity over CuPd@ZIF-8 (entry 1). In contrast, both the carbon−carbon triple bond and terminal aldehyde group are reduced over the CuPd catalyst (entry 2). This suggests that the small pore size of ZIF-8 allows the terminal aldehyde group only but restrains the internal triple bond to interact with the Pd sites. Therefore, the ZIF-8 shell

https://dx.doi.org/10.1021/acscatal.0c00177
ACS Catal. 2020, 10, 7753−7762

Table 1. Selective Hydrogenation of Different Alkynes over CuPd@ZIF-8[a]

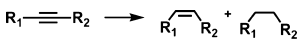

Entry	Substrate	Product	Con. (%)	Sel. (%)[c]
1			97	96
2	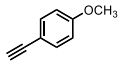	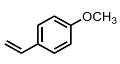	98	97
3	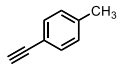	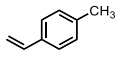	98	94
4	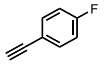	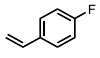	97	96
5	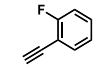		93	97
6	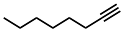	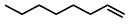	92	94
7	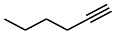	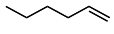	93	95
8	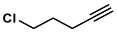	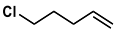	94	95
9[b]			95	97
10	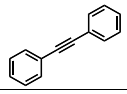	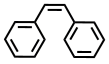	7	99

[a]Reaction conditions: substrate (0.1 mmol), time (5 min), CuPd@ZIF-8 (1 mg, Pd: 0.1 mol %), CH_3OH (6 mL), NH_3BH_3 (5 mg), light >400 nm, 160 mW/cm^2. [b]Time (10 min). [c]Catalytic reaction products were analyzed and identified by gas chromatography.

not only contributes to the stabilization of CuPd NCs but also offers the high regioselectivity via the space steric hindrance.

CONCLUSION

In summary, we have rationally fabricated a core−shell CuPd@ZIF-8 composite, featuring a cubic CuPd core and an MOF shell, for selective hydrogenation of alkynes. In the catalyst, the Cu not only achieves plasmonic photothermal conversion but also regulates the Pd electronic state to improve the catalytic chemoselectivity; the MOF stabilizes the CuPd NCs and enables regioselective hydrogenation of alkynes via the steric hindrance effect. Thanks to the well-dispersed Pd site, the Cu photothermal effect, and the *in situ* generated active hydrogen species from NH_3BH_3 that is well soluble in CH_3OH solvent, the hydrogenation of alkynes can be greatly boosted. Particularly, instead of traditional H_2 gas, the active hydrogen species generated from the alcoholysis of NH_3BH_3 ensure the high chemoselectivity in the hydrogenation of alkynes or alkene/alkyne mixture even over an extended reaction time. As a result, the CuPd@ZIF-8 is capable of catalyzing the hydrogenation of alkynes to alkenes with high chemo- and regioselectivity, good recyclability, and extremely high activity, featuring the highest TOF value reported thus far, toward phenylacetylene semihydrogenation. This work opens a new avenue to the rational design of highly efficient, chemo- and regioselective composite catalysts and suitable catalytic systems toward high-performance catalysis.

EXPERIMENTAL SECTION

Preparation of Cu Nanocubes. The Cu NCs were prepared according to the previous work with minor modifications.[51] Typically, 52.5 mg of $CuCl_2{\cdot}2H_2O$, 50 mg of glucose, 225 mg of HAD, and 25 mL of water were mixed in a 50 mL round-bottom flask and capped. The mixture solution was magnetically stirred at room temperature for 12 h. Then, the flask was transferred into an oil bath and heated at 100 °C for at least 6 h under magnetic stirring. As the reaction proceeded, the color of the solution was changing from blue to red-brown. After reaction, the product was harvested by centrifugation and washed six times with hot water (65 °C). Finally, the sample was dispersed into 5 mL of hot water (2 mg/mL).

Preparation of CuPd Nanocubes. The obtained Cu nanocube solution (1 mL) was diluted into 10 mL of deionized water in a 25 mL round-bottom flask, followed by the addition of 50 mg of PVP under vigorous stirring for 12 h. Then, 1 mL (0.91 M) of K_2PdCl_4 aqueous solution was injected into the Cu nanocube solution using a syringe pump at a rate of 0.25 mL/min under stirring for 12 h. After the galvanic reaction, the obtained product was collected via centrifugation and dispersed into 1 mL of methanol (2 mg/mL).

Preparation of CuPd@ZIF-8. Typically, the CuPd nanocube solution (1 mL) and the methanol solution of zinc nitrate (25 mM, 15 mL) were mixed at room temperature under N_2 bubbling for 5 min, and then, the equivalent volume of methanol solution of 2-methylimidazole (25 mM, 15 mL) was added to react at 40 °C for 30 min in a water bath with a N_2 balloon without stirring.[66] The resultant composite was collected by centrifugation and washed twice with methanol. The synthesized red-brown powder was further dried overnight at 333 K under dynamic vacuum and dispersed into 4 mL of methanol (1 mg/mL).

Table 2. Selective Hydrogenation of Phenylpropiolaldehyde over CuPd@ZIF-8 and CuPd[a]

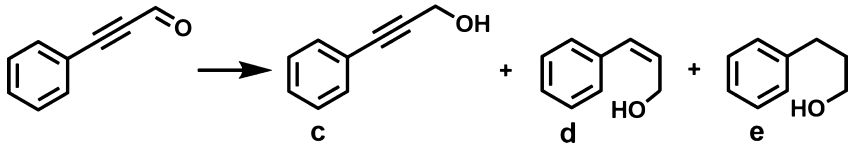

			yield[b] (%)		
entry	catalyst	conv. (%)	*c*	*d*	*e*
1	CuPd@ZIF-8	>99	98	2	
2	CuPd	>99	68	32	

[a]Reaction conditions: substrate (0.1 mmol), time (12 min), CuPd@ZIF-8 (Pd: 0.1 mol %), CuPd (Pd: 0.1 mol %), CH_3OH (4.5 mL), H_2O (1.5 mL), NH_3BH_3 (7.8 mg), light >400 nm, 160 mW/cm^2. [b]Catalytic reaction products were analyzed and identified by gas chromatography.

https://dx.doi.org/10.1021/acscatal.0c00177
ACS Catal. 2020, 10, 7753−7762

Preparation of Pd@ZIF-8. The Pd nanoparticles (~3 nm) were prepared first according to the reported work with minor modification.[67] Typically, 105 mg of PVP (~55 000 M_w), 60 mg of ascorbic acid, and 5 mg of KBr were dispersed into 8 mL of deionized water and preheated at 80 °C for 10 min. Then, 3 mL of K_2PdCl_4 (57 mg) aqueous solution was added and reacted for 3 h at 80 °C. The Pd nanoparticles were collected via centrifugation and washed with acetone five times. Finally, the obtained Pd nanoparticles are dispersed into 6 mL of deionized water (1 mg/mL). To synthesize Pd@ZIF-8, 750 μL of Pd nanoparticles solution (1 mg/mL) was mixed with the methanol solution of zinc nitrate ($Zn(NO_3)_2{\cdot}6H_2O$, 1.069 g, 15 mL), and then, the equivalent volume of methanol solution of 2-methylimidazole was added (2-MIM, 1.61 g, 15 mL). The obtained mixed solvent reacted for 10 h at room temperature. After the reaction, the gray powder was collected via centrifugation and washed three times with methanol. Finally, the obtained product was dried in vacuum oven at 60 °C for 12 h.

Preparation of ND_3BH_3 and NH_3BD_3. ND_3BH_3 was prepared according to the reported method with minor modifications.[68] First, 30 mg of NH_3BH_3 and 2 mL of CD_3OD were added in a 5 mL round-bottom flask and vigorously stirred for 4 h at room temperature; then, ND_3BH_3 was obtained after removing the solvent in vacuum. NH_3BD_3 was also prepared according to the reported method. Briefly, $NaBD_4$ (100 mg) and $(NH_4)_2SO_4$ (315.7 mg) were added to a 100 mL three-neck round-bottom flask. Then, 14 mL of THF was added, and the mixture was vigorously stirred at 40 °C for 2 h. Subsequently, it was cooled down to room temperature, filtered, and dried under vacuum to give NH_3BD_3 powder.

Photothermal Effect Evaluation. In general, a mixture of 1 mg of catalyst (1 mL, 1 mg/mL) and 6 mL of methanol was placed in a two-necked round-bottomed flask (25 mL) and capped. The mixture was irradiated under 160 mW/cm^2 light with a 300 W Xe lamp and magnetic stirring. Then, the temperature of solution was detected and recorded every 10 min to give the time−temperature curve.

Catalytic Performance Evaluation for the Dehydrogenation of Ammonia Borane (NH_3BH_3). In general, a mixture of 1 mg of catalyst (1 mL, 1 mg/mL) and 5 mL of methanol was placed in a two-necked round-bottomed flask (25 mL) and capped. The mixture was irradiated under 160 mW/cm^2 light with a 300 W Xe lamp. A gas buret filled with water was connected to the reaction flask to measure the volume of hydrogen evolved. The reaction started when NH_3BH_3 (5 mg) was added into the flask. The volume of the evolved hydrogen gas was monitored by recording the displacement of water in the gas buret. This reaction was completed when there was no more gas generated.

Catalytic Performance Evaluation of ZIF-8 and Pd@ZIF-8 for Hydrogenation of Phenylacetylene in the Presence of NH_3BH_3. Typically, a mixture of Pd@ZIF-8 or ZIF-8 (1 mg), 0.1 mmol of phenylacetylene, and 5 mL of methanol was placed in a two-necked round-bottomed flask (25 mL) under 160 mW/cm^2 light irradiation with a 300 W Xe lamp and mechanical stirring. Then, the reaction was initiated by adding 7.8 mg of NH_3BH_3.

Catalytic Performance Evaluation of CuPd@ZIF-8 or CuPd for Hydrogenation of Phenylacetylene and Phenylethylene in the Presence of NH_3BH_3. Typically, a mixture of 1 mg of CuPd@ZIF-8 (1 mL, 1 mg/mL), 0.1 mmol of phenylacetylene, and 5 mL of methanol was placed in a two-necked round-bottomed flask (25 mL) under 160 mW/cm^2 light irradiation with a 300 W Xe lamp and mechanical stirring. The reaction was initiated after adding 7.8 mg of NH_3BH_3 and proceeded for 10 min. After the reaction completion, 200 μL of the resultant mixture was taken into a mixed solvent with 1 mL of H_2O and 1 mL of ethyl acetate. Upon the adequate shaking, the mixture was allowed to be centrifuged, and the product was extracted to the upper layer of ethyl acetate. Then, 600 μL of sample in the upper solution was detected by GC. For the catalytic recycling experiments, CuPd@ZIF-8 was separated by centrifugation after reaction, being thoroughly washed by 5 mL of methanol 3 times. Then, it was dried in vacuum for 6 h for the next run. The hydrogenation of phenylethylene was attempted under similar conditions.

For the reaction with CuPd NCs, 5 mg of CuPd NCs was measured accurately and then dispersed into 5 mL of methanol, giving the CuPd solution with the concentration of ~1 mg/mL. Then, 16.5 μL of CuPd catalyst (1 mg/mL) was taken out and mixed with the 0.1 mmol of phenylacetylene and 5 mL of methanol in a two-necked round-bottomed flask (25 mL) under 160 mW/cm^2 light irradiation with a 300 W Xe lamp and mechanical stirring. The reaction was initiated after adding 7.8 mg of NH_3BH_3 and proceeded for 10 min. After the reaction completion, 200 μL of the resultant mixture was taken into a mixed solvent with 1 mL of H_2O and 1 mL of ethyl acetate. Upon adequate shaking, the mixture was allowed to be centrifuged, and the product was extracted to the upper layer of ethyl acetate. Then, 600 μL of sample in the upper solution was detected by GC.

Catalytic Performance Evaluation of CuPd@ZIF-8 for Hydrogenation of Phenylacetylene by H_2 Gas. The hydrogenation of phenylacetylene in the H_2 atmosphere was proceeded as follows. Typically, a mixture of 1 mg of CuPd@ZIF-8 (1 mL, 1 mg/mL), 0.1 mmol of phenylacetylene, and 5 mL of methanol was placed in a necked round-bottomed flask (25 mL) with a H_2 balloon. The reaction was accelerated under 160 mW/cm^2 light irradiation with a 300 W Xe lamp.

Catalytic Performance Evaluation of CuPd@ZIF-8 and CuPd for Hydrogenation of Phenylpropiolaldehyde in the Presence of NH_3BH_3. Typically, a mixture of CuPd@ZIF-8 (1 mL, 1 mg/mL) or an equimolar amount of CuPd (8.3 μL, 2 mg/mL), 0.1 mmol of phenylpropiolaldehyde, 4.5 mL of methanol, and 1.5 mL of H_2O was placed in a two-necked round-bottomed flask (25 mL) under 160 mW/cm^2 light irradiation with a 300 W Xe lamp and mechanical stirring. Then, the reaction was initiated by adding 7.8 mg of NH_3BH_3.

Time-Dependent Conversion of Phenylacetylene or Phenylethylene Hydrogenation. Typically, a mixture of 1 mg of CuPd@ZIF-8 (1 mL, 1 mg/mL), 0.1 mmol of phenylacetylene or phenylethylene, and 5 mL of methanol was placed in a two-necked round-bottomed flask (25 mL) under 160 mW/cm^2 light irradiation with a 300 W Xe lamp under mechanical stirring. Then, the reaction was initiated by adding 7.8 mg of NH_3BH_3. To obtain the kinetic curve of the catalytic reaction, during the reaction process, 80 μL of the reaction mixture was sampled per 30 s.

Dependency of the Reaction Rate on the Amount of NH_3BH_3. A mixture of 1 mg of CuPd@ZIF-8 (1 mL, 1 mg/mL), 0.1 mmol of phenylacetylene or phenylethylene, and 5 mL of methanol was placed in a two-necked round-bottomed flask (25 mL) under 160 mW/cm^2 light irradiation with a 300 W Xe lamp under mechanical stirring. Then, a different amount of NH_3BH_3 was added to initiate the reaction, and the

https://dx.doi.org/10.1021/acscatal.0c00177
ACS Catal. 2020, 10, 7753−7762

time-dependent conversion was completed following the above process, respectively.

Deuterium-Labeling Experiments. All controlled experiments were completed under the same conditions as the experiment above except that the substrate or reactant was replaced by the corresponding deuterated reagent.

DFT Calculation Method. The Perdew−Burke−Ernzerhof (PBE) functional and projector augmented wave (PAW) potentials were adopted to complete the DFT calculations by using the Vienna *ab initio* simulation package.[69,70] In detail, the spin polarization correction was included to consider the magnetism effect. Consistent with previous studies,[71,72] a 1 × 1 × 1 Γ-centered *k*-point and 500 eV cutoff energy were adopted to obtain accurate electronic energy in the ground-state. The convergence standards of energy and force were selected as 10^{-5} eV and 0.02 eV/Å. The vibrational frequency with finite displacements of ±0.02 Å was calculated to obtain the zero point energy correction and vibrational entropy correction.

■ ASSOCIATED CONTENT

Supporting Information

The Supporting Information is available free of charge at https://pubs.acs.org/doi/10.1021/acscatal.0c00177.

Materials and instrumentation; material characterizations; and catalytic results (PDF)

■ AUTHOR INFORMATION

Corresponding Author

Hai-Long Jiang − *Hefei National Laboratory for Physical Sciences at the Microscale, CAS Key Laboratory of Soft Matter Chemistry, Collaborative Innovation Center of Suzhou Nano Science and Technology, School of Chemistry and Materials Science, University of Science and Technology of China, Hefei, Anhui 230026, P. R. China;* orcid.org/0000-0002-2975-7977; Email: jianglab@ustc.edu.cn

Authors

Luyan Li − *Hefei National Laboratory for Physical Sciences at the Microscale, CAS Key Laboratory of Soft Matter Chemistry, Collaborative Innovation Center of Suzhou Nano Science and Technology, School of Chemistry and Materials Science, University of Science and Technology of China, Hefei, Anhui 230026, P. R. China*

Weijie Yang − *School of Energy and Power Engineering, North China Electric Power University, Baoding, Hebei 071003, P. R. China*

Qihao Yang − *Hefei National Laboratory for Physical Sciences at the Microscale, CAS Key Laboratory of Soft Matter Chemistry, Collaborative Innovation Center of Suzhou Nano Science and Technology, School of Chemistry and Materials Science, University of Science and Technology of China, Hefei, Anhui 230026, P. R. China*

Qiaoqiao Guan − *Hefei National Laboratory for Physical Sciences at the Microscale, CAS Key Laboratory of Soft Matter Chemistry, Collaborative Innovation Center of Suzhou Nano Science and Technology, School of Chemistry and Materials Science, University of Science and Technology of China, Hefei, Anhui 230026, P. R. China;* orcid.org/0000-0001-6968-8585

Junling Lu − *Hefei National Laboratory for Physical Sciences at the Microscale, CAS Key Laboratory of Soft Matter Chemistry, Collaborative Innovation Center of Suzhou Nano Science and Technology, School of Chemistry and Materials Science, University of Science and Technology of China, Hefei, Anhui 230026, P. R. China;* orcid.org/0000-0002-2607-6869

Shu-Hong Yu − *Hefei National Laboratory for Physical Sciences at the Microscale, CAS Key Laboratory of Soft Matter Chemistry, Collaborative Innovation Center of Suzhou Nano Science and Technology, School of Chemistry and Materials Science, University of Science and Technology of China, Hefei, Anhui 230026, P. R. China;* orcid.org/0000-0003-3732-1011

Complete contact information is available at: https://pubs.acs.org/10.1021/acscatal.0c00177

Author Contributions

The manuscript was written through contributions of all authors. All authors have given approval to the final version of the manuscript.

Notes

The authors declare no competing financial interest.

■ ACKNOWLEDGMENTS

We gratefully thank all reviewers for their insightful comments and valuable suggestions. This work was supported by the National Natural Science Foundation of China (21725101, 21871244, 21673213, 21521001), International Partnership Program of CAS (211134KYSB20190109), Fundamental Research Funds for the Central Universities (WK2060030029), and Fujian Institute of Innovation (CAS).

■ REFERENCES

(1) Studt, F.; Abild-Pedersen, F.; Bligaard, T.; Sørensen, R. Z.; Christensen, C. H.; Nørskov, J. K. Identification of Non-Precious Metal Alloy Catalysts for Selective Hydrogenation of Acetylene. *Science* **2008**, *320*, 1320−1322.

(2) Mitsudome, T.; Takahashi, Y.; Ichikawa, S.; Mizugaki, T.; Jitsukawa, K.; Kaneda, K. Metal-Ligand Core-Shell Nanocomposite Catalysts for the Selective Semihydrogenation of Alkynes. *Angew. Chem., Int. Ed.* **2013**, *52*, 1481−1485.

(3) Huang, F.; Deng, Y.; Chen, Y.; Cai, X.; Peng, M.; Jia, Z.; Ren, P.; Xiao, D.; Wen, X.; Wang, N.; Liu, H.; Ma, D. Atomically Dispersed Pd on Nanodiamond/Graphene Hybrid for Selective Hydrogenation of Acetylene. *J. Am. Chem. Soc.* **2018**, *140*, 13142−13146.

(4) Chinchilla, R.; Nájera, C. Chemicals from Alkynes with Palladium Catalysts. *Chem. Rev.* **2014**, *114*, 1783−1826.

(5) Li, G.; Jin, R. Gold Nanocluster-Catalyzed Semihydrogenation: A Unique Activation Pathway for Terminal Alkynes. *J. Am. Chem. Soc.* **2014**, *136*, 11347−11354.

(6) Albani, D.; Shahrokhi, M.; Chen, Z.; Mitchell, S.; Hauert, R.; Lopez, N.; Pérez-Ramírez, J. Selective Ensembles in Supported Palladium Sulfide Nanoparticles for Alkyne Semi-hydrogenation. *Nat. Commun.* **2018**, *9*, 2634.

(7) Trotus, I.-T.; Zimmermann, T.; Schüth, F. Catalytic Reactions of Acetylene: A Feedstock for the Chemical Industry Revisited. *Chem. Rev.* **2014**, *114*, 1761−1782.

(8) Yang, L.; Jin, Y.; Fang, X.; Cheng, Z.; Zhou, Z. Magnetically Recyclable Core-Shell Structured Pd-Based Catalysts for Semi-hydrogenation of Phenylacetylene. *Ind. Eng. Chem. Res.* **2017**, *56*, 14182−14191.

(9) Ji, S.; Chen, Y.; Zhao, S.; Chen, W.; Shi, L.; Wang, Y.; Dong, J.; Li, Z.; Li, F.; Chen, C.; Peng, Q.; Li, J.; Wang, D.; Li, Y. Atomically Dispersed Ruthenium Species Inside Metal-Organic Frameworks: Combining the High Activity of Atomic Sites and the Molecular Sieving Effect of MOFs. *Angew. Chem., Int. Ed.* **2019**, *58*, 4271−4275.

(10) Hoyt, C. B.; Sarazen, M. L.; Jones, C. W. Hydroboration of Substituted Alkynes using a Solid Polymeric Carboxylic Acid Catalyst. *J. Catal.* **2019**, *369*, 493−300.
(11) Kruppe, C. M.; Krooswyk, J. D.; Trenary, M. Selective Hydrogenation of Acetylene to Ethylene in the Presence of a Carbonaceous Surface Layer on a Pd/Cu (111) Single-Atom Alloy. *ACS Catal.* **2017**, *7*, 8042−8049.
(12) Cao, X.; Fu, Q.; Luo, Y. Catalytic Activity of Pd-Doped Cu Nanoparticles for Hydrogenation as a Single-Atom-Alloy Catalyst. *Phys. Chem. Chem. Phys.* **2014**, *16*, 8367−8375.
(13) Kyriakou, G.; Boucher, M. B.; Jewell, A. D.; Lewis, E. A.; Lawton, T. J.; Baber, A. E.; Tierney, H. L.; Flytzani-Stephanopoulos, M.; Sykes, E. C. H. Isolated Metal Atom Geometries as a Strategy for Selective Heterogeneous Hydrogenations. *Science* **2012**, *335*, 1209−1212.
(14) Pei, G. X.; Liu, X. Y.; Yang, X.; Zhang, L.; Wang, A.; Li, L.; Wang, H.; Wang, X.; Zhang, T. Performance of Cu-Alloyed Pd Single-Atom Catalyst for Semihydrogenation of Acetylene under Simulated Front-End Conditions. *ACS Catal.* **2017**, *7*, 1491−1500.
(15) da Silva, F. P.; Fiorio, J. L.; Goncalves, R. V.; Teixeira-Neto, E.; Rossi, L. M. Synergic Effect of Copper and Palladium for Selective Hydrogenation of Alkynes. *Ind. Eng. Chem. Res.* **2018**, *57*, 16209−16216.
(16) Guo, X.; Hao, C.; Jin, G.; Zhu, H.-Y.; Guo, X.-Y. Copper Nanoparticles on Graphene Support: An Efficient Photocatalyst for Coupling of Nitroaromatics in Visible Light. *Angew. Chem., Int. Ed.* **2014**, *53*, 1973−1977.
(17) Wang, F.; Li, C.; Chen, H.; Jiang, R.; Sun, L.-D.; Li, Q.; Wang, J.; Yu, J. C.; Yan, C.-H. Plasmonic Harvesting of Light Energy for Suzuki Coupling Reactions. *J. Am. Chem. Soc.* **2013**, *135*, 5588−5601.
(18) Liz-Marzán, L. M.; Murphy, C. J.; Wang, J. Nanoplasmonics. *Chem. Soc. Rev.* **2014**, *43*, 3820−3822.
(19) Chen, Y.-Z.; Wang, Z. U.; Wang, H.; Lu, J.; Jiang, H.-L. Singlet Oxygen-Engaged Selective Photo-Oxidation over Pt Nanocrystals/Porphyrinic MOF: The Roles of Photothermal Effect and Pt Electronic State. *J. Am. Chem. Soc.* **2017**, *139*, 2035−2044.
(20) Hung, L.-I.; Tsung, C.-K.; Huang, W.; Yang, P. Room-Temperature Formation of Hollow Cu_2O Nanoparticles. *Adv. Mater.* **2010**, *22*, 1910−1914.
(21) Sarkar, C.; Pendem, S.; Shrotri, A.; Dao, D. Q.; Mai, P. P. T.; Ngoc, T. N.; Chandaka, D. R.; Rao, T. V.; Trinh, Q. T.; Sherburne, M. P.; Mondal, J. Interface Engineering of Graphene-Supported Cu Nanoparticles Encapsulated by Mesoporous Silica for Size-Dependent Catalytic Oxidative Coupling of Aromatic Amines. *ACS Appl. Mater. Interfaces* **2019**, *11*, 11722−11735.
(22) Furukawa, H.; Cordova, K. E.; O'Keeffe, M.; Yaghi, O. M. The Chemistry and Applications of Metal-Organic Frameworks. *Science* **2013**, *341*, 1230444.
(23) Zhou, H.-C.; Kitagawa, S. Metal-Organic Frameworks (MOFs). *Chem. Soc. Rev.* **2014**, *43*, 5415−5418.
(24) Islamoglu, T.; Goswami, S.; Li, Z.; Howarth, A. J.; Farha, O. K.; Hupp, J. T. Postsynthetic Tuning of Metal-Organic Frameworks for Targeted Applications. *Acc. Chem. Res.* **2017**, *50*, 805−813.
(25) Li, B.; Wen, H.-M.; Cui, Y.; Zhou, W.; Qian, G.; Chen, B. Emerging Multifunctional Metal-Organic Framework Materials. *Adv. Mater.* **2016**, *28*, 8819−8860.
(26) Zhao, X.; Wang, Y.; Li, D.; Bu, X.; Feng, P. Metal-Organic Frameworks for Separation. *Adv. Mater.* **2018**, *30*, 1705189.
(27) Li, G.; Zhao, S.; Zhang, Y.; Tang, Z. Metal-Organic Frameworks Encapsulating Active Nanoparticles as Emerging Composites for Catalysis: Recent Progress and Perspectives. *Adv. Mater.* **2018**, *30*, 1800702.
(28) Kirchon, A.; Feng, L.; Drake, H. F.; Joseph, E. A.; Zhou, H.-C. From Fundamentals to Applications: a Toolbox for Robust and Multifunctional MOF Materials. *Chem. Soc. Rev.* **2018**, *47*, 8611−8638.
(29) Zhang, D.; Zhu, Y.; Liu, L.; Ying, X.; Hsiung, C.-E.; Sougrat, R.; Li, K.; Han, Y. Atomic-Resolution Transmission Electron Microscopy of Electron Beam-Sensitive Crystalline. *Science* **2018**, *359*, 675−679.
(30) Luo, Y.-H.; Dong, L.-Z.; Liu, J.; Li, S.-L.; Lan, Y.-Q. From Molecular Metal Complex to Metal-Organic Framework: The CO_2 Reduction Photocatalysts with Clear and Tunable Structure. *Coord. Chem. Rev.* **2019**, *390*, 86−126.
(31) Rungtaweevoranit, B.; Baek, J.; Araujo, J. R.; Archanjo, B. S.; Choi, K. M.; Yaghi, O. M.; Somorjai, G. A. Copper Nanocrystals Encapsulated in Zr-based Metal-Organic Frameworks for Highly Selective CO_2 Hydrogenation to Methanol. *Nano Lett.* **2016**, *16*, 7645−7649.
(32) Yang, Q.; Xu, Q.; Yu, S.-H.; Jiang, H.-L. Pd Nanocubes@ZIF-8: Integration of Plasmon-Driven Photothermal Conversion with a Metal-Organic Framework for Efficient and Selective Catalysis. *Angew. Chem., Int. Ed.* **2016**, *55*, 3685−3689.
(33) Zhang, W.; Zheng, B.; Shi, W.; Chen, X.; Xu, Z.; Li, S.; Chi, Y. R.; Yang, Y.; Lu, J.; Huang, W.; Huo, F. Site-Selective Catalysis of a Multifunctional Linear Molecule: The Steric Hindrance of Metal-Organic Framework Channels. *Adv. Mater.* **2018**, *30*, 1800643.
(34) Li, X.; Zhang, B.; Tang, L.; Goh, T. W.; Qi, S.; Volkov, A.; Pei, Y.; Qi, Z.; Tsung, C.-K.; Stanley, L.; Huang, W. Cooperative Multifunctional Catalysts for Nitrone Synthesis: Platinum Nanoclusters in Amine-Functionalized Metal-Organic Frameworks. *Angew. Chem., Int. Ed.* **2017**, *56*, 16371−16375.
(35) Yang, Q.; Xu, Q.; Jiang, H.-L. Metal-Organic Frameworks Meet Metal Nanoparticles: Synergistic Effect for Enhanced Catalysis. *Chem. Soc. Rev.* **2017**, *46*, 4774−4808.
(36) Huang, Y.-B.; Liang, J.; Wang, X.-S.; Cao, R. Multifunctional Metal-Organic Framework Catalysts: Synergistic Catalysis and Tandem Reactions. *Chem. Soc. Rev.* **2017**, *46*, 126−157.
(37) Hu, P.; Morabito, J. V.; Tsung, C.-K. Core-Shell Catalysts of Metal Nanoparticle Core and Metal-Organic Framework Shell. *ACS Catal.* **2014**, *4*, 4409−4419.
(38) Rogge, S. M. J.; Bavykina, A.; Hajek, J.; Garcia, H.; Olivos-Suarez, A. I.; Sepulveda-Escribano, A.; Vimont, A.; Clet, G.; Bazin, P.; Kapteijn, F.; Daturi, M.; Ramos-Fernandez, E. V.; Llabres, I. X. F. X.; Van Speybroeck, V.; Gascon, J. Metal-Organic and Covalent Organic Frameworks as Single-Site Catalysts. *Chem. Soc. Rev.* **2017**, *46*, 3134−3184.
(39) Zhao, M.; Ou, S.; Wu, C.-D. Porous Metal-Organic Frameworks for Heterogeneous Biomimetic Catalysis. *Acc. Chem. Res.* **2014**, *47*, 1199−1207.
(40) Lee, K. J.; Lee, J. H.; Jeoung, S.; Moon, H. R. Transformation of Metal-Organic Frameworks/Coordination Polymers into Functional Nanostructured Materials: Experimental Approaches Based on Mechanistic Insights. *Acc. Chem. Res.* **2017**, *50*, 2684−2692.
(41) Khaletskaya, K.; Reboul, J.; Meilikhov, M.; Nakahama, M.; Diring, S.; Tsujimoto, M.; Isoda, S.; Kim, F.; Kamei, K. I.; Fischer, R. A.; Kitagawa, S.; Furukawa, S. Integration of Porous Coordination Polymers and Gold Nanorods into Core-Shell Mesoscopic Composites toward Light-Induced Molecular Release. *J. Am. Chem. Soc.* **2013**, *135*, 10998−11005.
(42) Wang, C.; An, B.; Lin, W. Metal-Organic Frameworks in Solid-Gas Phase Catalysis. *ACS Catal.* **2019**, *9*, 130−146.
(43) Zhai, Q.; Bu, X.; Zhao, X.; Li, D.; Feng, P. Pore Space Partition in Metal-Organic Frameworks. *Acc. Chem. Res.* **2017**, *50*, 407−417.
(44) Hermes, S.; Schröter, M.-K.; Schmid, R.; Khodeir, L.; Muhler, M.; Tissler, A.; Fischer, R. W.; Fischer, R. A. Metal@ MOF: Loading of Highly Porous Coordination Polymers Host Lattices by Metal Organic Chemical Vapor Deposition. *Angew. Chem., Int. Ed.* **2005**, *44*, 6237−6241.
(45) Liu, H.; Chang, L.; Bai, C.; Chen, L.; Luque, R.; Li, Y. Controllable Encapsulation of "Clean" Metal Clusters within Mofs Through Kinetic Modulation: towards Advanced Heterogeneous Nanocatalysts. *Angew. Chem., Int. Ed.* **2016**, *55*, 5019−5023.
(46) Dhakshinamoorthy, A.; Garcia, H. Catalysis by Metal Nanoparticles Embedded on Metal-Organic Frameworks. *Chem. Soc. Rev.* **2012**, *41*, 5262−5284.
(47) Zhao, M.; Yang, K.; Wang, Y.; Li, G.; Guo, J.; Gu, L.; Hu, W.; Zhao, H.; Tang, Z. Metal-Organic Frameworks as Selectivity Regulators for Hydrogenation Reactions. *Nature* **2016**, *539*, 76−80.

https://dx.doi.org/10.1021/acscatal.0c00177
ACS Catal. 2020, 10, 7753−7762

(48) Choe, K.; Zheng, F.; Wang, H.; Yuan, Y.; Zhao, W.; Xue, G.; Qiu, X.; Ri, M.; Shi, X.; Wang, Y.; Li, G.; Tang, Z. Fast and Selective Semihydrogenation of Alkynes by Palladium Nanoparticles Sandwiched in Metal-Organic Frameworks. *Angew. Chem., Int. Ed.* **2020**, *59*, 3650−3657.
(49) Park, K. S.; Ni, Z.; Côté, A. P.; Choi, J. Y.; Huang, R.; Uribe-Romo, F. J.; Chae, H. K.; O'Keeffe, M.; Yaghi, O. M. Exceptional Chemical and Thermal Stability of Zeolitic Imidazolate Frameworks. *Proc. Natl. Acad. Sci. U. S. A.* **2006**, *103*, 10186−10191.
(50) Huang, X.-C.; Lin, Y.-Y.; Zhang, J.-P.; Chen, X.-M. Ligand-Directed Strategy for Zeolite-Type Metal-Organic Frameworks: Zinc (II) Imidazolates with Unusual Zeolitic Topologies. *Angew. Chem., Int. Ed.* **2006**, *45*, 1557−1559.
(51) Jin, M.; He, G.; Zhang, H.; Zeng, J.; Xie, Z.; Xia, Y. Shape-Controlled Synthesis of Copper Nanocrystals in an Aqueous Solution with Glucose as a Reducing Agent and Hexadecylamine as a Capping Agent. *Angew. Chem., Int. Ed.* **2011**, *50*, 10560−10564.
(52) McCue, A. J.; McRitchie, C. J.; Shepherd, A. M.; Anderson, J. A. Cu/Al_2O_3 Catalysts Modified with Pd for Selective Acetylene Hydrogenation. *J. Catal.* **2014**, *319*, 127−135.
(53) Rodríguez-Kessler, P. L.; Alonso-Dávila, P.; Navarro-Santos, P.; Morato-Márquez, J. A.; Ortíz-Chi, F.; Rodríguez-Domínguez, A. R. Hydrogen Chemisorption on Pd-Doped Copper Clusters. *J. Phys. Chem. C* **2019**, *123*, 15834−15840.
(54) Zhan, W.-W.; Zhu, Q.-L.; Xu, Q. Dehydrogenation of Ammonia Borane by Metal Nanoparticle Catalysts. *ACS Catal.* **2016**, *6*, 6892−6905.
(55) Demirci, U. B.; Miele, P. Sodium Borohydride versus Ammonia Borane, in Hydrogen Storage and Direct Fuel Cell Applications. *Energy Environ. Sci.* **2009**, *2*, 627−637.
(56) He, T.; Pachfule, P.; Wu, H.; Xu, Q.; Chen, P. Hydrogen Carrier. *Nat. Rev. Mater.* **2016**, *1*, 16059.
(57) Yang, Q.; Chen, Y.-Z.; Wang, Z. U.; Xu, Q.; Jiang, H.-L. One-Pot Tandem Catalysis over Pd@MIL-101: Boosting the Efficiency of Nitro Compound Hydrogenation by Coupling with Ammonia Borane Dehydrogenation. *Chem. Commun.* **2015**, *51*, 10419−10422.
(58) Shen, M.; Liu, H.; Yu, C.; Yin, Z.; Muzzio, M.; Li, J.; Xi, Z.; Yu, Y.; Sun, S. Room-Temperature Chemoselective Reduction of 3-Nitrostyrene to 3-Vinylaniline by Ammonia Borane over Cu Nanoparticles. *J. Am. Chem. Soc.* **2018**, *140*, 16460−16463.
(59) Han, C.; Meng, P.; Waclawik, E. R.; Zhang, C.; Li, X.-H.; Yang, H.; Antonietti, M.; Xu, J. Palladium/Graphitic Carbon Nitride (g-C_3N_4) Stabilized Emulsion Microreactor as a Store for Hydrogen from Ammonia Borane for Use in Alkene Hydrogenation. *Angew. Chem., Int. Ed.* **2018**, *57*, 14857−14861.
(60) Fu, S.; Chen, N.-Y.; Liu, X.; Shao, Z.; Luo, S.-P.; Liu, Q. Ligand-Controlled Cobalt-Catalyzed Transfer Hydrogenation of Alkynes: Stereodivergent Synthesis of Z- and E-Alkenes. *J. Am. Chem. Soc.* **2016**, *138*, 8588−8594.
(61) Rej, S.; Madasu, M.; Tan, C.-S.; Hsia, C.-F.; Huang, M. H. Polyhedral Cu_2O to Cu Pseudomorphic Conversion for Stereoselective Alkyne Semihydrogenation. *Chem. Sci.* **2018**, *9*, 2517−2524.
(62) Mitsudome, T.; Yamamoto, M.; Maeno, Z.; Mizugaki, T.; Jitsukawa, K.; Kaneda, K. One-Step Synthesis of Core-Gold/Shell-Ceria Nanomaterial and Its Catalysis for Highly Selective Semihydrogenation of Alkynes. *J. Am. Chem. Soc.* **2015**, *137*, 13452−13455.
(63) Li, Z.; He, T.; Liu, L.; Chen, W.; Zhang, M.; Wu, G.; Chen, P. Covalent Triazine Framework Supported Non-Noble Metal Nanoparticles with Superior Activity for Catalytic Hydrolysis of Ammonia Borane: from Mechanistic Study to Catalyst Design. *Chem. Sci.* **2017**, *8*, 781−788.
(64) Vasilikogiannaki, E.; Titilas, I.; Vassilikogiannakis, G.; Stratakis, M. *cis*-Semihydrogenation of Alkynes with Amine Borane Complexes Catalyzed by Gold Nanoparticles under Mild Conditions. *Chem. Commun.* **2015**, *51*, 2384−2387.
(65) Finšgar, M.; Jackson, J. Application of Corrosion Inhibitors for Steels in Acidic Media for the Oil and Gas Industry: A Review. *Corros. Sci.* **2014**, *86*, 17−41.
(66) Chen, L.; Peng, Y.; Wang, H.; Gu, Z.; Duan, C. Synthesis of Au@ ZIF-8 Single- or Multi-Core-Shell Structures for Photocatalysis. *Chem. Commun.* **2014**, *50*, 8651−8654.
(67) Jin, M.; Liu, H.; Zhang, H.; Xie, Z.; Liu, J.; Xia, Y. Synthesis of Pd Nanocrystals Enclosed by {100} Facets and with Sizes < 10 nm for Application in CO Oxidation. *Nano Res.* **2011**, *4*, 83−91.
(68) Cantelli, R.; Paolone, A.; Palumbo, O.; Leardini, F.; Autrey, T.; Karkamkar, A.; Luedtke, A. T. Rotational Dynamics in Ammonia Borane: Evidence of Strong Isotope Effects. *J. Alloys Compd.* **2013**, *580*, S63−S66.
(69) Perdew, J. P.; Burke, K.; Ernzerhof, M. Generalized Gradient Approximation Made Simple. *Phys. Rev. Lett.* **1996**, *77*, 3865−3868.
(70) Kresse, G.; Furthmüller, J. Efficiency of Ab-Initio Total Energy Calculations for Metals and Semiconductors Using A Plane-Wave Basis Set. *Comput. Mater. Sci.* **1996**, *6*, 15−50.
(71) Gao, Z. Y.; Yang, W. J.; Ding, X. L.; Lv, G.; Yan, W. P. Support Effects on Adsorption and Catalytic Activation of O_2 in Single Atom Iron Catalysts with Graphene-Based Substrates. *Phys. Chem. Chem. Phys.* **2018**, *20*, 7333−7341.
(72) Yang, W.; Gao, Z.; Liu, X.; Li, X.; Ding, X.; Yan, W. Single-Atom Iron Catalyst with Single-Vacancy Graphene-Based Substrate as A Novel Catalyst for NO Oxidation: A Theoretical Study. *Catal. Sci. Technol.* **2018**, *8*, 4159−4168.

https://dx.doi.org/10.1021/acscatal.0c00177
ACS Catal. 2020, 10, 7753−7762